

Dust from AGBs: relevant factors and modelling uncertainties

P. Ventura¹, F. Dell’Agli^{1,3}, R. Schneider¹, M. Di Criscienzo^{1,2}, C. Rossi³,
F. La Franca⁴, S. Gallerani⁵, R. Valiante¹

¹INAF – Osservatorio Astronomico di Roma, Via Frascati 33, 00040, Monte Porzio Catone (RM), Italy

²INAF – Osservatorio Astronomico di Capodimonte, Salita Moiarello 16, 80131, Napoli, Italy

³Dipartimento di Fisica, Università di Roma “La Sapienza”, P.le Aldo Moro 5, 00143, Roma, Italy

⁴Dipartimento di Matematica e Fisica, Università degli Studi “Roma Tre”, Via della Vasca Navale 84, 00146, Roma, Italy

⁵Scuola Normale Superiore, Piazza dei Cavalieri 7, 56126 Pisa, Italy

Accepted, Received; in original form

ABSTRACT

The dust formation process in the winds of Asymptotic Giant Branch stars is discussed, based on full evolutionary models of stars with mass in the range $1M_{\odot} \leq M \leq 8M_{\odot}$, and metallicities $0.001 < Z < 0.008$. Dust grains are assumed to form in an isotropically expanding wind, by growth of pre-existing seed nuclei.

Convection, for what concerns the treatment of convective borders and the efficiency of the schematization adopted, turns out to be the physical ingredient used to calculate the evolutionary sequences with the highest impact on the results obtained.

Low-mass stars with $M \leq 3M_{\odot}$ produce carbon type dust with also traces of silicon carbide. The mass of solid carbon formed, fairly independently of metallicity, ranges from a few $10^{-4}M_{\odot}$, for stars of initial mass $1 - 1.5M_{\odot}$, to $\sim 10^{-2}M_{\odot}$ for $M \sim 2 - 2.5M_{\odot}$; the size of dust particles is in the range $0.1\mu\text{m} \leq a_C \leq 0.2\mu\text{m}$. On the contrary, the production of silicon carbide (SiC) depends on metallicity. For $10^{-3} \leq Z \leq 8 \times 10^{-3}$ the size of SiC grains varies in the range $0.05\mu\text{m} < a_{\text{SiC}} < 0.1\mu\text{m}$, while the mass of SiC formed is $10^{-5}M_{\odot} < M_{\text{SiC}} < 10^{-3}M_{\odot}$.

Models of higher mass experience Hot Bottom Burning, which prevents the formation of carbon stars, and favours the formation of silicates and corundum. In this case the results scale with metallicity, owing to the larger silicon and aluminium contained in higher- Z models. At $Z = 8 \times 10^{-3}$ we find that the most massive stars produce dust masses $m_d \sim 0.01M_{\odot}$, whereas models of smaller mass produce a dust mass ten times smaller. The main component of dust are silicates, although corundum is also formed, in not negligible quantities ($\sim 10 - 20\%$).

Key words: Stars: abundances – Stars: AGB and post-AGB. ISM: abundances, dust

1 INTRODUCTION

During the last years the evolution experienced by stars of intermediate mass after the consumption of central helium has received a growing interest by the astrophysical community. This phase, known as Asymptotic Giant Branch (AGB, Iben & Renzini 1983; Lattanzio & Boothroyd 1987; Herwig 2005), is much shorter than the previous stages of core hydrogen and helium burning, but is extremely important for the role played by these sources in the pollution of the interstellar medium. During the AGB evolution the stars lose all their external mantle, returning into the interstellar medium material whose chemical composition was altered by internal nuclear processes.

AGBs have been suggested as the main contributors to the pollution of the interstellar medium in Globular Clusters, giving rise to the formation of multiple populations (Ventura et al. 2001). The gas ejected by AGBs, possibly diluted with pristine gas, may stimulate the formation of one or more additional stellar components, overlapped to the original population present in the cluster (D’Ercole et al. 2008, 2010). This scenario can explain most of the observational data, such as the chemical anomalies involving light elements (Gratton et al. 2012) and the photometric features of the main sequence and of the horizontal branch of Globular Clusters (Piotto 2009).

The interest towards AGBs stems also from the physical conditions of their circumstellar envelopes, particularly

suitable to gas condensation into dust grains. The surface layers of these stars are sufficiently cool ($T_{\text{eff}} < 4000\text{K}$) to allow dust formation at typical distances of 3–10 stellar radii from the surface, where the densities are still sufficiently large ($\rho > 10^{-14}\text{gr/cm}^3$, Gail & Sedlmayr 1985) to allow formation of meaningful quantities of dust.

Dust formation is a complex phenomenon, which is strongly interfaced with the dynamical and thermal structure of the winds of this class of objects (Bertschinger & Chevalier 1985; Wood 1979; Bowen 1988). Stellar pulsation is known to trigger the formation of periodic shocks, that favours the increase in the local density, thus stimulating gas condensation in cool regions in the stellar surroundings. Radiation pressure on dust grains is currently believed as the dominant mechanism triggering mass loss in these structures (Fleischer et al. 1992).

A self-consistent description of the dust formation process would require full coupling of results from stellar evolution modelling with the description of the wind. A natural outcome of such a treatment would be the outwards velocity of gas and dust particles leaving the star, thus the mass loss rate experienced. Because we are still far from achieving this target, the few models available in the literature treat the wind independently, based on the results coming from the integration of the equations of stellar equilibrium, from which the values of luminosity, effective temperature and mass loss rate of the star are obtained (Ferrarotti & Gail 2001, 2002, 2006). These studies may be considered as a preliminary step towards a more complete treatment, where central object and external wind are described simultaneously.

The reliability of the results obtained, in terms of the amount of dust formed, is hampered by the uncertainties associated to the wind model, for what concerns, e.g., the initial velocity of gas particles, the opacities relevant to determine the radiation pressure on grains, the sticking coefficients of each dust species (Ferrarotti & Gail 2006; Ventura et al. 2012a,b).

AGB modelling is also relevant for the results obtained. The type of grains formed, either silicates or carbonaceous particles, depends on the description of the processes able to alter the surface chemistry of AGBs, i.e. Third Dredge-Up (TDU) and Hot Bottom Burning (HBB). The efficiency of either mechanisms is affected by the modelling of convection and in particular by the treatment of the convective/radiative interface (Herwig 2000, 2005) and of the temperature gradient in regions unstable to convective motions (Ventura & D’Antona 2005a). The description of mass loss is also extremely relevant, because it has a direct impact on the AGB evolutionary time scale (Ventura & D’Antona 2005b); furthermore, the mass loss rate determines the density profile of the wind, thus the amount of dust formed.

It is for all these reasons that results in the literature presented by different research groups, though using the same description of the wind and of the dust grains formation and growth, differ considerably in the mass and composition of dust formed (Ferrarotti & Gail 2006; Ventura et al. 2012a,b; Di Criscienzo et al. 2013; Nanni et al. 2013).

The scope of this work is to discuss how the properties of dust formed in the winds of AGBs depend on the implementation of some fundamental features of the model, namely: i) the macrophysics adopted to describe the AGB

evolution; ii) the thermodynamical description of the wind; iii) the formation and growth of grains.

We present a new grid of dust formation models assuming stellar metallicities of $Z=4 \times 10^{-3}$, which fills the gap among the chemistries of our previous explorations, i.e. $Z=10^{-3}$ (Ventura et al. 2012a), $Z=8 \times 10^{-3}$ (Ventura et al. 2012b), $Z=3 \times 10^{-4}$ (Di Criscienzo et al. 2013). This allows to explore in details the role played by the chemical composition in the dust formation process. Also, this metallicity will enable to compare model predictions with observational data in the Small Magellanic Cloud (Larsen et al. 2000) and in metal-rich galactic Globular Clusters (Carretta et al. 2009).

In addition to our previous investigations on this topic, we present AGB models of different metallicities where i) some extra-mixing is assumed from any convective border (including the base of the external mantle); ii) the description of mass loss is based on hydrodynamical wind models including carbon-dust formation (Wachter et al. 2008).

The paper is organized as follows: in section 2 we present an overview of the status of the art of the modelling of dust formation around AGBs; sections 3 and 4 describe the inputs used to model the AGB evolution of stars and the dust grain growth in the expanding winds; carbon dust formation is discussed in section 5, whereas silicates production in more massive AGBs experiencing HBB is presented in section 6; finally, section 7 is devoted to an overall discussion of the results obtained.

2 DUST FORMATION MODELLING AROUND AGBS: STATUS OF THE ART

The pioneering explorations by the Heidelberg group (Ferrarotti & Gail 2001, 2002, 2006) set the framework to describe the dust formation process in the winds of AGBs. The wind is assumed to expand isotropically from the surface of the star, moving with velocities of a few km/s, entering into the dust formation layer, where gas (and dust) particles are accelerated via radiation pressure on the newly formed grains.

The dust grains are assumed to grow owing to the gas molecules impinging on the already formed solid particles. The rate at which the grains grow scales with the density of the gas; this defines a very narrow region where dust formation occurs. An asymptotic behaviour is reached, with the wind expanding outwards with large velocities (typically $\sim 10 - 50$ km/s).

This is a simplified view of a much more complex situation, where large amplitude pulsations trigger periodic shocks (Wood 1979; Bowen 1988; Bertschinger & Chevalier 1985): gas particles, rather than expanding at constant velocity, are projected on ballistic trajectories, where they contribute to the increase in the local density in regions very cool, thus extremely suitable to dust formation (Fleischer et al. 1992). A complete, self-consistent treatment would require the simultaneous description of the periodic variation of the stellar properties and of the structure of the wind, such that condensation takes place in the regions where the shock favours the increase in the density. A natural outcome of such a treatment would be the determination of the mass loss rate, via the density and the

velocities of the gas leaving the star (Wachter et al. 2002, 2008; Mattsson et al. 2008).

Such a self-consistent approach is still missing and the models currently available treat the wind independently, assuming as inputs the physical parameters of the central star, i.e. effective temperature, luminosity, mass loss rate and the surface chemical composition. The most relevant shortcoming of this approach is the lack of any feedback between the formation of dust grains and the mass loss rate, which is assumed *a priori*; we will come back to this point in the following.

Because the structure of the wind is based on the properties of the central star, the effective temperature (T_{eff}), luminosity (L) and mass loss rate (\dot{M}) are key quantities in determining the amount of dust formed. Condensation of gas molecules is favoured at low T_{eff} 's, because smaller temperatures in the wind allows the dust forming region to be closer to the surface of the star, in higher density zones. Larger values of \dot{M} favour dust formation, because mass conservation requires the density in the wind to increase linearly with \dot{M} (see Eq. 2 below). Luminosity has no direct impact on the dust formation process, but it affects the acceleration due to radiation pressure, which scales with L (Eq. 5 and 6 below).

The surface chemistry of the star is relevant in determining which kind of dust is formed. The CO molecule has an extremely large dissociation energy (11eV), which means that the least abundant between carbon and oxygen is bound in CO molecules. In C-rich environments there is no oxygen available, thus the only dust that can be formed is solid carbon, silicon carbide (SiC) and iron (Groenewegen et al. 1998). When the C/O ratio is below unity all the carbon present is locked into CO: silicates, iron and corundum can form (Ossenkopf et al. 1992).

The physical evolution of AGBs, and of their surface chemistry, depends on some fundamental physical properties such as convection and mass loss (Herwig 2005; Karakas 2011).

The treatment of the convective instability is the largest uncertainty affecting stellar evolution models. Owing to the lack of a self-consistent theory of turbulence, the transport of energy within regions unstable to convective motions is treated parametrically. The mixing length Λ , the typical scale of convective motions, is assumed to be proportional to the pressure scale height H_p : $\Lambda = \alpha H_p$. The parameter α is calibrated to reproduce the current radius of the Sun; with the latest updates in the micro-physics adopted, recent investigations give $\alpha_{\odot} = 1.75$ (Bressan et al. 2012).

The AGB phase is the most sensitive to the convection model adopted. Models based on the Full Spectrum of Turbulence (FST, Canuto & Mazzitelli 1991) evolve at larger luminosities, on more expanded configurations, in comparison with their counterparts calculated with the traditional Mixing Length Theory (Ventura & D'Antona 2005a). FST models loose their envelopes more rapidly, and experience on the average a smaller number of thermal pulses (TP).

The efficiency of the convective model adopted has also an important feedback on the Hot Bottom Burning phenomenon, in models with mass $M \geq 3 - 3.5 M_{\odot}$: the base of the convective envelope becomes sufficiently hot ($T \geq 40$ MK) to favour an advanced proton capture nucleosynthesis, with the destruction of the surface carbon,

and, when the temperatures exceed ~ 70 MK, the depletion of oxygen and the production of Aluminium via activation of the Mg-Al chain. HBB is found in all models with core mass above $\sim 0.8 M_{\odot}$ when convection is modelled according to the FST formulation. Also MLT models with $\alpha > \alpha_{\odot}$ achieve much more easily HBB conditions (Renzini & Voli 1981; Boothroyd & Sackmann 1988a). The ignition of HBB is accompanied by the increase in the luminosity (Blöcker & Schönberner 1991), which, in turn, triggers the increase in the mass loss rate.

In models experiencing HBB the production of silicates is greatly favoured: the C-star stage is inhibited by the destruction of the surface carbon, and the star evolves at large luminosities, loose mass at a high rate, which increase the dust formation rate.

Low-mass AGBs (M below $3 M_{\odot}$) do not reach HBB conditions, independently of convection modelling. In these stars the only mechanism able to alter the surface chemistry is the Third Dredge-Up, which gradually enriches the surface in carbon, eventually making C/O to exceed unity. Initially, when the mass loss rate is small and the C-star stage is not yet reached, small quantities of silicates are produced; in the final evolutionary stages carbon dust is produced in great quantities, owing to the large surface carbon abundances and the high mass loss rates experienced.

While there is a general consensus on the sequence of events given above, the amount of carbon dust formed is still matter of debate, because the evolutionary stage at which the star becomes a C-star and the extent of the surface carbon enrichment depend on the inwards penetration of the convective envelope during the TDU (see discussion in Karakas 2011). This is rendered uncertain by the poor knowledge of the behaviour of convective eddies near the convective/radiative interface, particularly of the extent of the extra-mixing, i.e. the distance they travel within radiatively stable regions. The extra-mixing from convective cores of stars in central burning phases can be calibrated via comparison with the observed main sequences of open clusters (Vandenbergh et al. 2006), by analysis of binary star data (Claret 2007), and asteroseismological investigations (Briquet et al. 2007; Montalbán et al. 2013). The situation for the AGB phase is more complex, as there is no observable that allows a straight calibration of the overshoot from the base of the envelope, and from the boundaries of the shell which forms at the ignition of each TP. The most widely argument used so far is the reproduction of the carbon star luminosity function in the Magellanic Clouds, which allows to determine the core mass at which TDU begins, and the extent of the inwards penetration of the convective envelope (Izzard et al. 2004; Marigo & Girardi 2007). These information can be used to estimate the extension of the mixed regions within the AGBs interiors. The larger is the extra-mixing, the more carbon dust is produced, because more and more carbon is dredged-up to the surface regions.

The description of the mass loss mechanism is also extremely relevant in determining the evolution of AGBs (Herwig 2005). The rate at which AGBs loose mass determines the duration of the whole evolutionary phase (Ventura & D'Antona 2005b), but has also important consequences on the modification of the surface chemistry. In massive AGBs, experiencing HBB, the mass loss rate is strictly correlated with the degree of p-capture nucleosynthesis at the

bottom of the surface envelope: lower rates allow a stronger nucleosynthesis, thus larger changes in the abundances of the elements involved in the CNO, Ne–Na and Mg–Al cycles. In the low-mass regime, large rates favour faster consumption of the envelope: the star undergoes a smaller number of TPs, thus the carbon surface enrichment is reduced.

This has a strong impact on the dust formation in the circumstellar envelopes. A direct effect of the mass loss description is associated with the higher density of the winds when the mass loss is large, which enhance dust production. Also, as stated above, mass loss changes the surface chemical composition, and the mass fractions of those elements relevant to allow dust formation (e.g. carbon for carbon-type dust): this clearly changes the amount of dust which can be formed.

3 STELLAR EVOLUTION MODELLING

The evolutionary sequences presented here were computed by means of the ATON code for stellar evolution. The interested reader may find in Ventura et al. (1998) a detailed description of the numerical structure of the code. The most recent updates can be found, e.g., in Ventura & D’Antona (2009). We recall here the main physical inputs, most relevant for the topic of the present investigation.

3.1 Convection

The arguments presented in the previous section outline how relevant the description of convection is for the AGB phase, in terms of the evolution of the main physical quantities, number of thermal pulses experienced, change in the surface chemical composition due to HBB and TDU.

In agreement with other investigations by our group, the temperature gradient within convective regions is found by the FST model, developed by Canuto & Mazzitelli (1991).

Mixing of chemicals and nuclear burning were coupled with a diffusive approach, according to the scheme suggested by Cloutman & Eoll (1976). The overshoot of convective eddies into radiatively stable regions is described by an exponential decay of the velocity v beyond the formal border found via the Schwarzschild criterion. The relation used is

$$v = v_b \times \exp\left(\pm \frac{1}{\zeta} \log \frac{P}{P_b}\right) \quad (1)$$

where the argument of the exponential is taken positive for overshoot from the upper border of the convective zone, whereas the minus sign is used for overshoot below the convective region. v_b and P_b are the values of velocity and pressure at the formal boundary. The extent of the overshoot is given by the free parameter ζ .

For the convective cores that form during the hydrogen and helium burning phases, and generally for the phases previous the AGB evolution, we followed the calibration given in Ventura et al. (1998), and assumed $\zeta = 0.02$.

For what concerns the AGB phase, we calibrated the extent of the extra-mixing from the base of the convective envelope and from the borders of the shell that forms at the ignition of each thermal pulse based on the luminosity function (LF) of carbon stars in the Large Magellanic Cloud

(Groenewegen 2004). We find that adopting $\zeta = 0.002$ leads to a satisfactory agreement between the observed and the predicted LFs. With this assumption we recover the relation between initial mass and luminosity of the transition from O-rich to C-rich surface chemical composition given in Marigo & Girardi (2007).

3.2 Mass loss

In agreement with our previous explorations focused on the AGB evolution, we use for the phases preceeding the C-star stage the formulation by Blöcker (1995). The Blöcker formula ($\dot{M} \propto M^{-3.1} \times R \times L^{3.7}$, where M , R and L are, respectively, the stellar mass, radius and luminosity) is suitable to describe the steep increase of \dot{M} with luminosity that characterizes massive AGBs; however, it underestimates the mass loss suffered by C-stars, because it is based on a description of the circumstellar envelope of MIRA variables that neglects the carbon-dust formation process, and the radiation pressure on dust grains, which induces a great acceleration of the wind. To describe the C-star phase we rely on the formulation by Wachter et al. (2008), giving the mass loss rates experienced by low-mass AGBs as a function of mass, luminosity and effective temperature. The expression used is $\dot{M} \propto M^\alpha T_{eff}^\beta L^\gamma$, where typical values for the exponents (partly depending on the metallicity) are $\alpha \sim -3$, $\beta \sim -7$, $\gamma \sim +3$.

3.3 Radiative opacities

The radiative opacities k for temperatures above 10^4 K were calculated using the OPAL online tool (Iglesias & Rogers 1996); for smaller temperatures we used the AESOPUS tool described in Marigo & Aringer (2009). This choice allows to account for the increase in the opacity associated with the change in the surface chemistry determined by TDU. The pioneering study by Marigo (2002) shows how the modelling of AGBs experiencing TDU is sensitive to the set of opacities adopted; detailed discussions on this argument can be found in Ventura & Marigo (2009, 2010).

3.4 Chemical composition

The new models presented in this work have metallicity $Z=0.004$, initial helium $Y=0.26$; the mixture is alpha-enhanced, with $[\alpha/Fe] = +0.2$. A discussion of their main physical properties, and of the change in the surface chemistry determined by TDU and HBB, can be found in Ventura et al. (2013b). Here we focus on the dust formed in their surroundings.

In addition to this new grid, we also present updated models for stellar metallicities $Z=0.001$, $Z=0.008$ (discussed in previous papers) obtained with the new implementation of the extra-mixing from convective regions during the AGB phase and the mass loss description of the C-star phase.

4 DUST GRAINS GROWTH

The structure of the wind and the dust formation process is described following the schematization by Ferrarotti & Gail (2006). As discussed in the introduction, the thermodynamic

structure of the wind and the dust formation process are entirely determined by the physical and chemical conditions at the surface of the central star. The latter is assumed to evolve independently of the properties of the wind: this is possible because the mass loss rate is determined via a parametric recipe, rather than by full coupling of star's and wind's descriptions.

4.1 Thermodynamic structure of the wind

The wind is assumed to expand isotropically from the surface of the star, described by a mass M , luminosity L , radius R , and effective temperature T_{eff} . The thermodynamic structure of the wind is set by the relations giving the variation of density (ρ) and temperature (T) with the distance r from the center of the star.

Indicating with \dot{M} the rate of mass loss, we have

$$\dot{M} = 4\pi r^2 \rho v, \quad (2)$$

where v is the velocity of the wind.

The temperature of the gas in the wind decreases with r according to the relation given by Lucy (1976)

$$T = \frac{1}{2} T_{\text{eff}}^4 \left[1 - \sqrt{1 - \frac{R^2}{r^2}} + \frac{3}{2} \tau \right]. \quad (3)$$

The optical depth entering Eq.3 is found by the differential equation

$$\frac{d\tau}{dr} = -\rho k \frac{R^2}{r^2}. \quad (4)$$

The boundary condition for Eq.4 is that τ vanishes at infinity (for numerical reasons, we impose that this condition is reached at a distance of $10^4 R$ from the centre, where the asymptotic behaviour of all the quantities is definitively reached).

The model is completed by the description of the acceleration of dust particles under the effects of gravitational attraction from the star and radiation pressure on dust grains:

$$\frac{dv}{dr} = -\frac{GM}{r^2} \times (1 - \Gamma), \quad (5)$$

with

$$\Gamma = \frac{kL}{4\pi cGM}. \quad (6)$$

For the wind velocity, we assume that it enters the dust forming region with a constant velocity $v_0 = 1$ km/sec, and is accelerated by radiation pressure. When dust formation is efficient, the results show only a modest dependence on the assumed value for v_0 .

4.2 Dust grains formation and growth

The system of equations given above can be closed if we know the opacity coefficient k , needed to find Γ (Eq.6), and the optical depth (Eq.4). k can be found by summing the gas and dust contributions. The former is calculated by means

of the AESOPUS tool, whereas for the latter we calculate the individual contributions from the various dust species formed.

In a carbon-rich context the species of dust formed are solid carbon, iron and silicon carbide, whereas for M stars we consider the formation of silicates (olivine, pyroxene and quartz), solid iron and corundum. This latter species was not present in our previous investigations.

For each species it is defined a key-element, the least abundant among the elements present in the molecules concurring to the condensation process (see Table 1 for the details of the formation reactions of the various dust species considered). The abundance of the key-element in the wind is extremely relevant for the amount of dust of a given species that can be formed, because the growth rate (J_i^{gr}) of the grains scales with the number density of the key-species, whereas the destruction rate (J_i^{dec}) is proportional to the vapour pressure of the molecule containing the key-element in equilibrium with the solid particles.

The growth of the grain size of species i is calculated via the equation

$$\frac{da_i}{dt} = V_{0,i} (J_i^{\text{gr}} - J_i^{\text{dec}}), \quad (7)$$

where $V_{0,i}$ is the volume of the nominal molecule in the solid.

The vapour pressures needed to estimate the decay rates J_i^{dec} were found by calculating the free enthalpy of formation of the molecules involved. Most of the computations are based on the release by Sharp & Huebner (1990), with the only exceptions of carbon and SiC, that were kindly provided by Prof. Gail (private communication). Following Ferrarotti & Gail (2006), we do not consider any destruction reaction for solid carbon, but we assume that it can form only at temperatures below 1100K.

The growth rates J_i^{gr} are proportional to the sticking coefficients α_i of the molecule including the key-elements on the solid grains. The choice of various coefficients is the same as in our previous investigations. For corundum, owing to lack of laboratory data, we explore the range 0.1–1.

The composition of olivine and pyroxene depends on the relative fraction of magnesium and iron, indicated, respectively, with x and $1 - x$ (see Table 1). The magnesium percentages in the olivine (x_{ol}) and pyroxene (x_{py}) dust particles are found via the equations

$$\frac{dx_{\text{ol}}}{dt} = \frac{3V_{0,\text{ol}}}{a_{\text{ol}}} \left[(x_g - x_{\text{ol}}) J_{\text{ol}}^{\text{gr}} + \frac{1}{2} (J_+^{\text{ex}} - J_-^{\text{ex}}) \right] \quad (8)$$

$$\frac{dx_{\text{py}}}{dt} = \frac{3V_{0,\text{py}}}{a_{\text{py}}} \left[(x_g - x_{\text{py}}) J_{\text{py}}^{\text{gr}} + \frac{1}{2} (J_+^{\text{ex}} - J_-^{\text{ex}}) \right] \quad (9)$$

where x_g is defined as the relative gas abundance of magnesium with respect to the Mg+Fe sum.

The quantity $(J_+^{\text{ex}} - J_-^{\text{ex}})$ gives the difference between the exchange rate of iron by magnesium per unit surface area during collisions of Mg with the grain surface and the rate of the reverse reaction, and is defined as in Gail & Sedlmayr (1999).

The amount of dust formed is indicated by the fraction of gas condensed into solid grains. This is expressed by the fraction f_i of the key-element that is in the solid state. We have

Table 1. Dust species considered in the present analysis, their formation reaction and the corresponding key elements (see text).

Grain Species	Formation Reaction	Key element	Sticking coefficient
Olivine	$2x\text{Mg} + 2(1-x)\text{Fe} + \text{SiO} + 3\text{H}_2\text{O} \rightarrow \text{Mg}_{2x}\text{Fe}_{2(1-x)}\text{SiO}_4 + 3\text{H}_2$	Si	0.1
Pyroxene	$x\text{Mg} + (1-x)\text{Fe} + \text{SiO} + 2\text{H}_2\text{O} \rightarrow \text{Mg}_x\text{Fe}_{(1-x)}\text{SiO}_3 + 2\text{H}_2$	Si	0.1
Quartz	$\text{SiO} + \text{H}_2\text{O} \rightarrow \text{SiO}_2(s) + \text{H}_2$	Si	0.1
Corundum	$2\text{AlO} + \text{H}_2\text{O} \rightarrow \text{Al}_2\text{O}_3 + \text{H}_2$	Al	0.1-1
Silicon Carbide	$2\text{Si} + \text{C}_2\text{H}_2 \rightarrow 2\text{SiC} + \text{H}_2$	Si	1
Carbon	$\text{C} \rightarrow \text{C}(s)$	C	1
Iron	$\text{Fe} \rightarrow \text{Fe}(s)$	Fe	1

$$f_i = \frac{4\pi(a_i^3 - a_{0,i}^3)}{3V_{0,i}} \frac{\epsilon_d}{\epsilon_i}, \quad (10)$$

where $a_{0,i}$ is the initial size of the seed nuclei in the wind, ϵ_i is the number density of the key-elements in the wind, normalized to the hydrogen density, and ϵ_d is the normalized density of the seed nuclei.

We assumed for each species $a_{0,i} = 0.01\mu\text{m}$; the final results are independent of this assumption, provided that a minimum amount of dust, sufficient to accelerate the wind, is formed.

The situation for ϵ_d is more tricky. The typical number densities of grains in the outflow of M-stars of solar metallicity has been determined observationally, and is of the order of 10^{-13} (Knapp 1985). The situation for C-stars and for M-stars of different metallicity could be different (see the discussion in Nanni et al., 2013), but presently any choice for ϵ_d would have a large degree of arbitrariness.

The opacity coefficient is found via the equation

$$k = k_{\text{gas}} + \sum_i f_i k_i \quad (11)$$

where the k_i 's are the opacity coefficients for the various dust species formed. The optical constants used to determine the opacities are the same as in Ventura et al. (2012a).

The coupled system of differential equations for the wind and the dust formation of the various species is solved with an Adams-Bashforth integrator (Golub & Ortega 1992). The equations are solved in the radial outward direction. All the r.h.s. of eqs. 7 are set to zero until the first dust species become stable.

5 CARBON DUST PRODUCTION IN AGBS

5.1 Current uncertainties from AGB modelling

Models with $M \leq 3M_\odot$ form silicates at the beginning of the AGB evolution, whereas in more advanced phases repeated TDU episodes lead to $\text{C}/\text{O} > 1$. The surface carbon enrichment depends on the treatment of convective borders, particularly on the extension of the extra-mixed region: this zone is stable, based on the Schwarzschild criterium, yet it is reached by convective eddies, that cross the convective/radiative interface, pushed by inertia.

Locating the borders of convection zones during the AGB phase is one of the long-standing problems in the context of stellar evolution (Mowlavi 1999). Certain trends

have been identified by extant models, such as the increase in the extent of TDU in lower metallicity models (Boothroyd & Sackmann 1988b), and the fact that TDU ceases when the mass of the envelope drops below a threshold value (Straniero et al. 1997). Yet the extension of mixed zones is still unknown from first principles: comparison with the observations of carbon stars in the Galaxy (Wallerstein & Knapp 1998) and in the Magellanic Clouds (Bessel et al. 1983) indicate that standard models, where mixing is allowed only within zones satisfying the Schwarzschild criterium, fail to reproduce the observed patterns, and that some extra-mixing is required.

The presence of extra-mixing favours the increase in the surface carbon, for two reasons: a) overshoot from the bottom of the convective envelope during the inwards penetration that follows the thermal pulse makes more carbon-rich matter to be mixed with the surface layers; b) extra-mixing from the borders of the convective shell that forms during each TP increases the strength of the pulse, in turn increasing the extent of the inwards penetration of the convective envelope (Herwig & Austin 2004).

Previous investigations fixed the conditions for TDU to occur either by imposing the temperature of the innermost layer reached by the penetration of the convective mantle (Marigo et al. 1999), or by assuming a relation between the core mass at which TDU begins as a function of mass and metallicity (Karakas et al. 2002; Izzard et al. 2004; Marigo & Girardi 2007). In our case the most straightforward way of introducing some overshoot is by assuming a non vanishing value of ζ (see Eq. 1).

The impact of assuming some extra-mixing on dust production during the AGB phase was discussed on qualitative grounds in Ventura et al. (2012b), by analysing the role played by ζ (see Eq. 1); no calibration of the extra-mixing was given. In this paper we use $\zeta = 0.002$, according to the calibration of ζ aimed at reproducing the luminosity function of carbon stars in the Magellanic Clouds, given in section 3.1¹.

The effects of extra-mixing are shown in Fig. 1, where we compare the results obtained with no extra-mixing (blue, dashed tracks), with those found with $\zeta = 0.002$ (red, dotted). We will refer to these models as *noov* and *over*, respec-

¹ It is not surprising that this value is a factor 10 smaller than the ζ used to describe overshoot from convective cores during the H-burning phase, given the different physical conditions in the two cases, and the much shorter duration of each individual TDU, compared to the time scales of core H-burning.

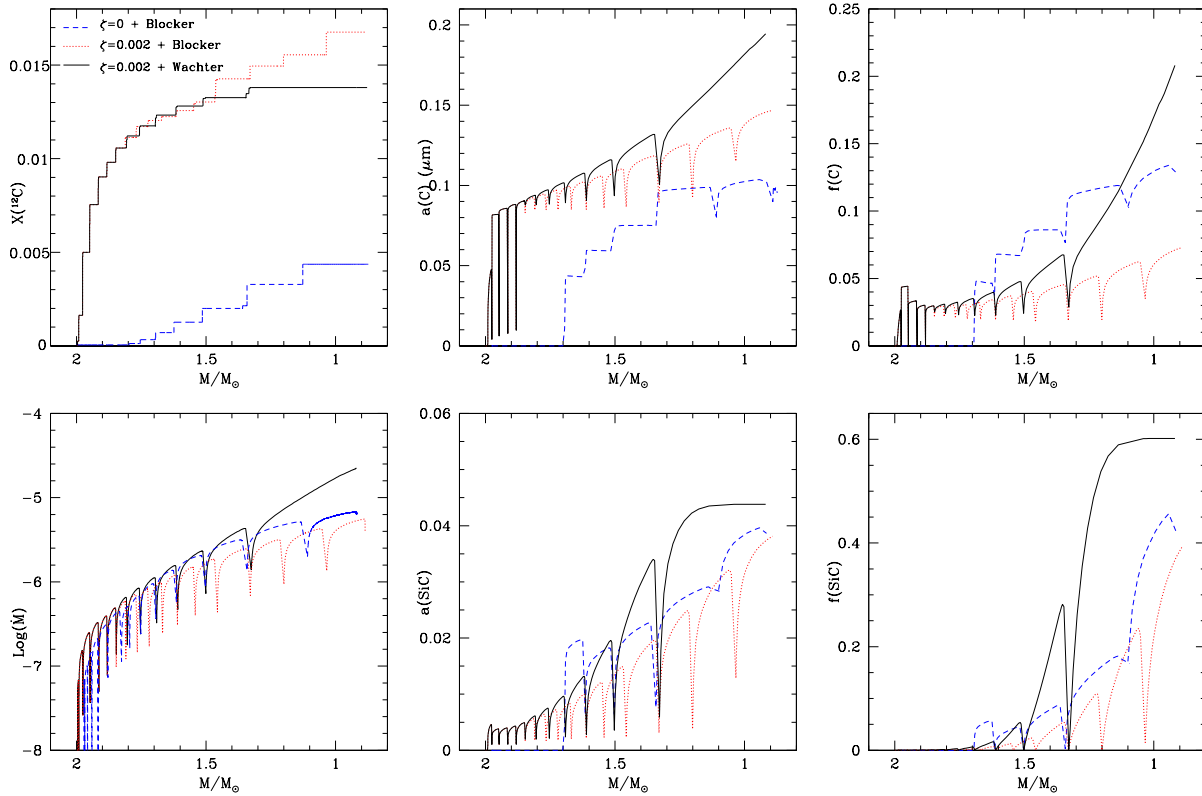


Figure 1. The variation during the AGB evolution of a model of initial mass $2M_{\odot}$, of metallicity $Z=0.001$ (Ventura et al. 2012a). In the abscissa we indicate the current mass of the star, decreasing during the evolution. In the top panels we show the carbon surface mass fraction (left), the grains size of solid carbon dust particles (middle), and the fraction of gaseous carbon condensed into dust (right). In the bottom panel we report the mass loss rate (left), the size of SiC grains (middle), and the fraction of silicon condensed into SiC dust. The models calculated with the Blöcker mass loss rate with no extra-mixing and with $\zeta = 0.002$ are indicated, respectively, with blue, dashed lines and with red, dotted tracks. The black, solid lines indicate models with the mass loss description by Wachter et al. (2008).

tively. The figure refers to the evolution of a $2M_{\odot}$ model of metallicity $Z=0.001$, published in Ventura et al. (2012a).

In the upper, left panel, we see that the carbon increase is much more pronounced in the *over* model: the surface carbon reaches a final mass fraction of $X(C) \sim 0.017$, a factor ~ 3 larger than in the *noov* case. This has a straight consequence on the production of solid carbon, as we see in the upper, middle panel, showing the variation of the solid carbon size in the two cases: the size of carbon grains formed in the *over* model approaches $a_C \sim 0.15\mu\text{m}$, whereas in the *noov* case they barely reach $a_C \sim 0.1\mu\text{m}$. Carbon dust formation occurs at an earlier phase in the *over* model, because TDU is more efficient in favouring the transition from M- to C-star; in the *noov* case, the star loses $0.2M_{\odot}$ before the condition $C/O > 1$ is reached.

The fraction of carbon condensed into dust (right, upper panel) is larger in the *noov* case, owing to the smaller amount of carbon available at the surface.

The quantity of silicon carbide formed is less sensitive to the treatment of convective borders, as shown in the middle and right, lower panels of Fig. 1. This is because the key-element for SiC is silicon, whose surface content is independent of the efficiency of TDU. Clearly production of SiC demands that the C-star stage has already been achieved,

thus SiC grains start to form in earlier phases in the *over* model.

To discuss the role played by the description of mass loss, we compare the results obtained with the treatment based on the Blöcker’s formula with the more recent compilation by Wachter et al. (2008). This latter is more suitable to describe the mass loss mechanism in these evolutionary phases, as it is based on simulations of stellar winds driven by radiation pressure on carbon grains. The rates by Wachter et al. (2008) show a great sensitivity to the effective temperature of the star, and show a rapid increase in the rate of mass loss as soon as carbon–dust formation begins.

The results obtained with the Wachter et al. (2008) formula are indicated in Fig. 1 with black, solid, tracks. We used the same prescription of the extra-mixing from convective borders as for the *over* case, thus we can analyse the role of mass loss treatment by comparing with the red, dotted lines in the six panels of Fig. 1.

The mass loss rate given by the Wachter et al. (2008) formula are larger once the C-star stage is reached, as can be seen in the left, bottom panel: the star experiences a smaller number of TPs, thus the surface carbon enrichment (shown in the left, upper panel) is lower. Despite the lower carbon available, more dust is formed: this is due to the

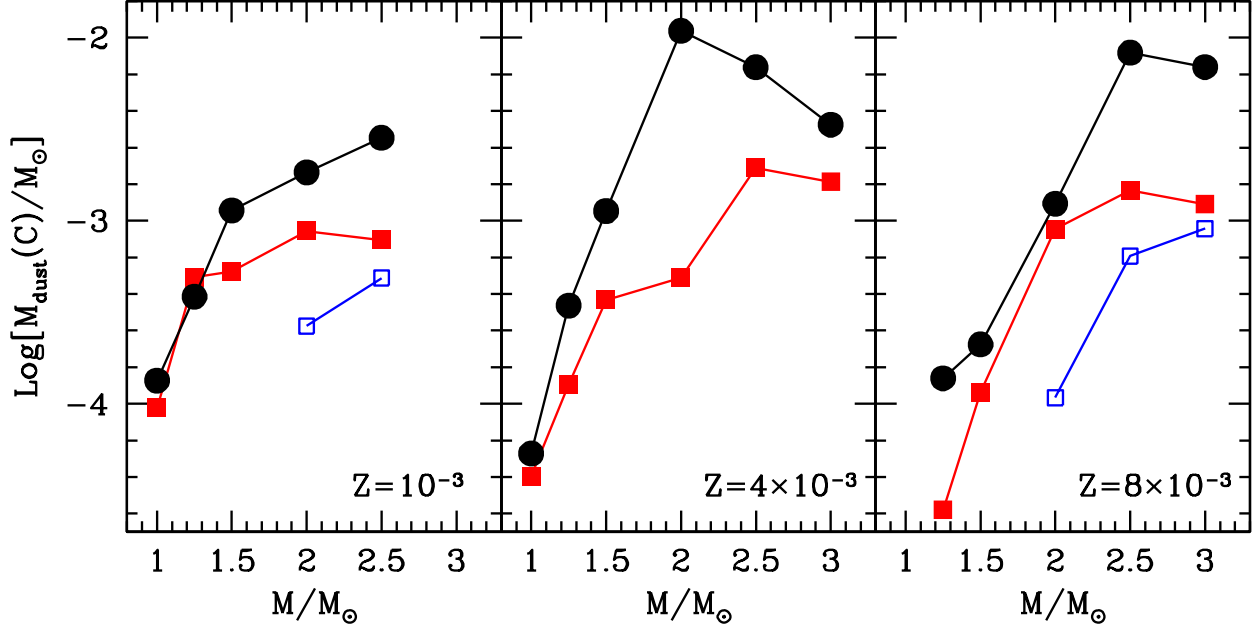


Figure 2. Mass of solid carbon produced as a function of the initial mass of the star for the metallicities $Z = 10^{-3}$ (left), $Z = 4 \times 10^{-3}$ (middle), $Z = 8 \times 10^{-3}$ (right). The meanings of the symbols is as follows. Blue, open squares: no-overshoot models with the Blöcker description of mass loss, published in Ventura et al. (2012a,b); Red, full squares: $\zeta = 0.002$ models (Blöcker's mass loss); Black, full circles: $\zeta = 0.002$ models with the Wachter et al. (2008) mass loss.

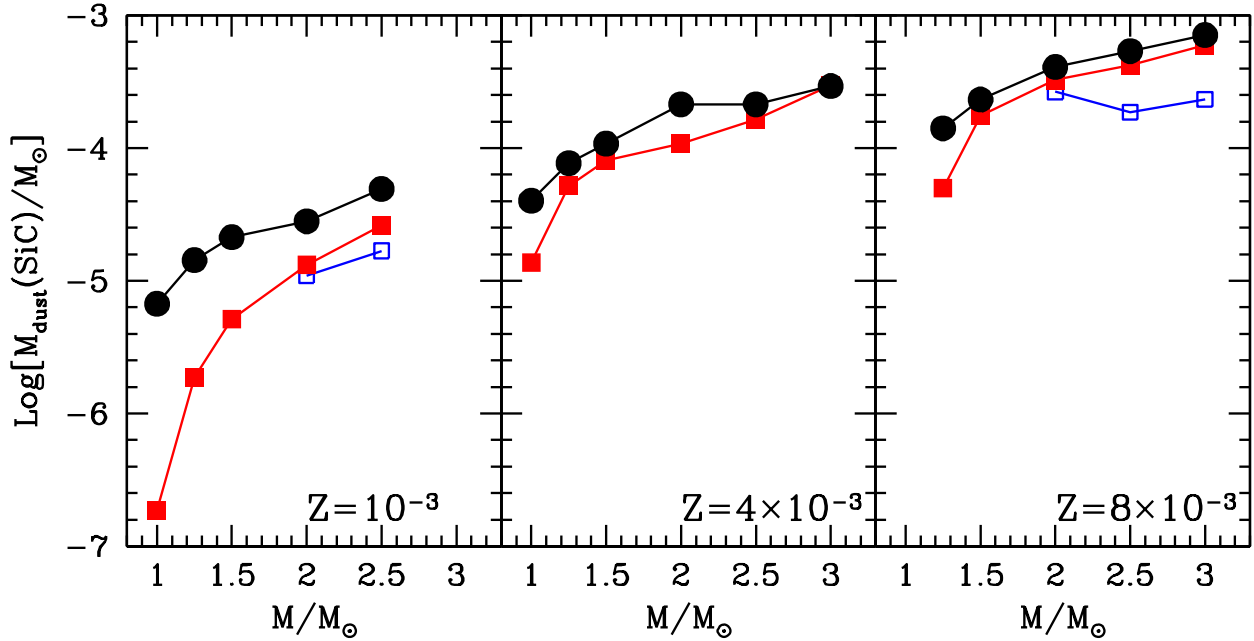


Figure 3. Mass of silicon carbide produced by AGB models of different initial mass. The three panels refer to results for $Z = 10^{-3}$ (left), $Z = 4 \times 10^{-3}$ (middle) and $Z = 8 \times 10^{-3}$ (right). The meaning of the symbols is the same as in Fig. 2.

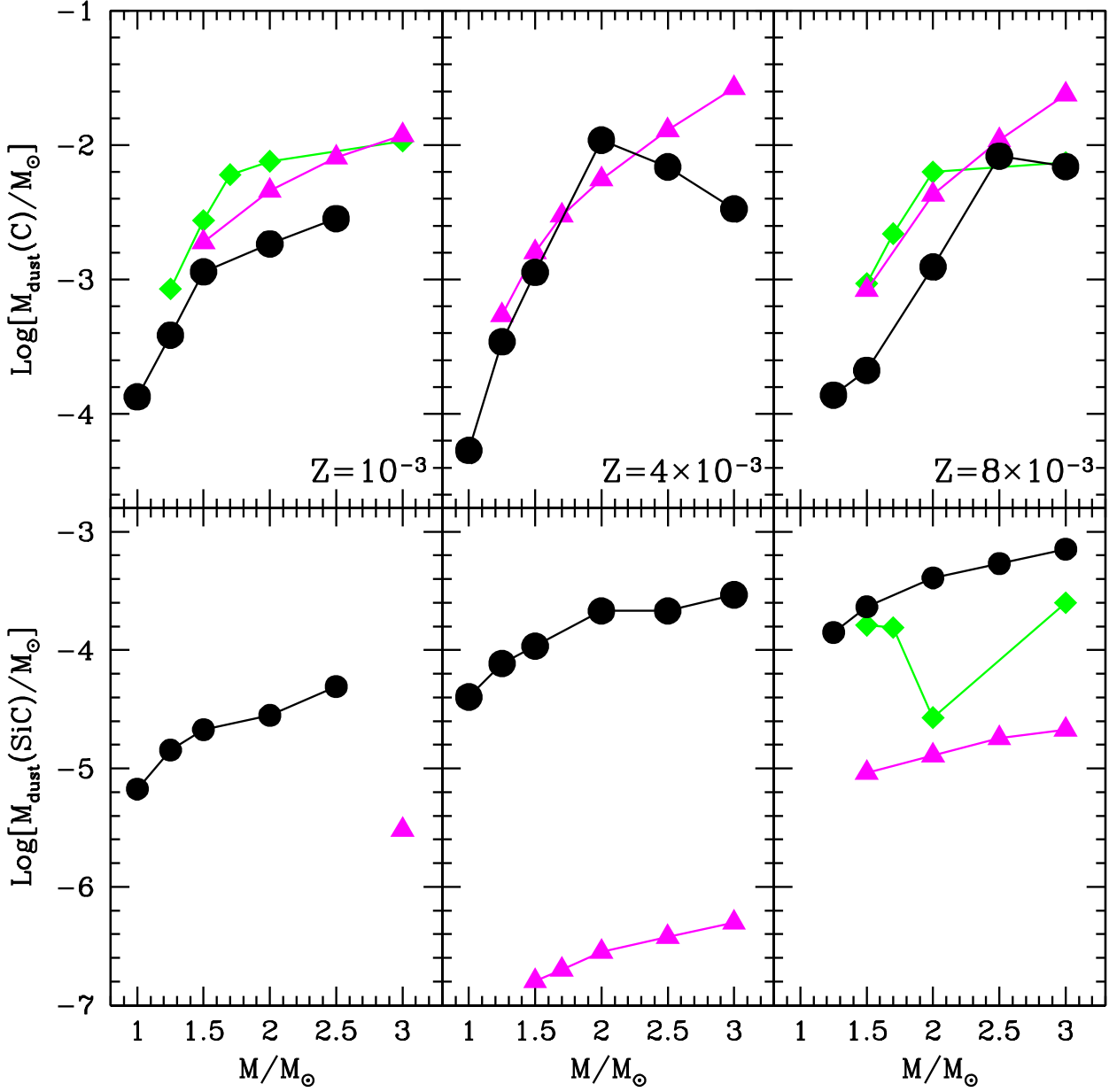


Figure 4. The comparison among the mass of solid carbon (top panels) and SiC (bottom) produced by AGB models of various initial mass and metallicities $Z=10^{-3}$ (left), $Z=4 \times 10^{-3}$ (middle), $Z=8 \times 10^{-3}$ (right). The meaning of the symbols is as follows: Black circles: models with mass loss by Wachter et al. (2008) and $\zeta = 0.002$; Magenta triangles: models by Ferrarotti & Gail (2006); Green diamonds: models by Nanni et al. (2013).

larger density of the wind, favoured by the higher mass loss rate.

We see in the middle, bottom panel that the higher \dot{M} also favours a greater production of SiC.

The overall comparison among results obtained with the different assumptions concerning the convective borders and the mass loss mechanism are shown in Fig. 2 (solid carbon produced) and in Fig. 3 (silicon carbide). The three panels refer to the metallicities $Z=10^{-3}$ (left), $Z=4 \times 10^{-3}$ (middle), $Z=8 \times 10^{-3}$ (right). Part of the results concerning $Z=10^{-3}$

and $Z=8 \times 10^{-3}$ were published in Ventura et al. (2012a,b). Here we extend the computations to models calculated with the mass loss by Wachter et al. (2008), and to the metallicity $Z=4 \times 10^{-3}$; for this latter Z the case $\zeta = 0$ with no extra-mixing was not explored.

In the $Z=10^{-3}$ case we see that when extra-mixing is neglected only models of initial mass $M=2, 2.5M_{\odot}$ become carbon stars and produce solid carbon. Use of the mass loss rate by Wachter et al. (2008) favours a larger dust production for $M \geq 1.5M_{\odot}$. For smaller masses the effect of the

higher mass loss rates is counterbalanced by the lower carbon available, such that the results turn out to be approximately independent of the mass loss description.

The $Z=4 \times 10^{-3}$ models show a similar behaviour, the impact of mass loss increasing for larger masses. The amount of solid carbon produced (and also the differences determined by the mass loss treatment) reaches a maximum around for stars of initial mass around $2, 2.5M_{\odot}$, and becomes progressively smaller as the mass increases, and approaches the threshold limit for HBB ignition.

At $Z=8 \times 10^{-3}$, similarly to $Z=10^{-3}$, we find that when no overshoot is considered only models with $M \geq 2M_{\odot}$ produce solid carbon. Use of the mass loss prescription by Wachter et al. (2008) favours an increase in the total solid carbon produced of almost one order of magnitude for masses above $\sim 2M_{\odot}$. For smaller masses the differences are negligible, because use of the Wachter et al. (2008) formula favours a rapid loss of the envelope as soon as the C-star is achieved, which prevents further carbon to be dredged-up to the surface.

Fig. 3 shows that the production of silicon carbide is also dependent on the treatment of convective borders and the description of mass loss. The results are easier to be interpreted in this case, owing to the approximately constant value of the key-element, i.e. silicon, which, unlike carbon, is not changed by TDU.

Models using the mass loss treatment by Wachter et al. (2008) produce more silicon carbide, owing to the higher density in the wind. Clearly models with no overshoot produce a smaller amount of SiC, because they reach the C-star stage in later phases, after part of the envelope was lost.

5.2 The comparison with other investigations

We compare the results by Ferrarotti & Gail (2006), and the more recent investigation by Nanni et al. (2013) with our models. This comparison is aimed to stress the differences in the AGB modelling, because the three studies use the same description of the thermodynamics of the wind and of the dust formation process.

In Fig. 4 we indicate the results by Ferrarotti & Gail (2006) and Nanni et al. (2013), respectively, with magenta, full triangles and green, solid diamonds. The comparison for $Z=4 \times 10^{-3}$ is limited to Ferrarotti & Gail (2006), as this metallicity was not discussed by Nanni et al. (2013).

In all cases the amount of carbon dust formed increases with mass, because more massive stars experience more thermal pulses, dredge-up more carbon at the surface, and also loose the external envelope at a higher rate, which increases the number density of gas particles in the wind.

For $Z=10^{-3}$ the carbon dust produced by our models for $M \geq 2M_{\odot}$ is a factor of ~ 3 smaller compared to Ferrarotti & Gail (2006). The interpretation of such a difference is not straightforward, because the models by Ferrarotti & Gail (2006) are based on a synthetic modelling, and keep the same efficiency of TDU until the latest AGB phases, when the mass of the envelope is greatly reduced. Also, in our models we account for the modification of the surface chemistry in the computation of the low-temperature opacities via the AESOPUS tool (Marigo & Aringer 2009): this leads to a general cooling of the outer layers, which, in turn, favours the expansion of the

external regions, a higher mass loss rate, and a faster consumption of the stellar envelope, before a great enrichment of surface carbon can be achieved (Ventura & Marigo 2009, 2010). The smaller densities of carbon nuclei is probably the main reason for the lower amount of solid carbon produced by our models (Ventura et al. 2012a).

The comparison with the results by Nanni et al. (2013) also shows that the carbon dust produced by our models is lower, although the differences are smaller than with Ferrarotti & Gail (2006). These can be ascribed to the choice of the initial density of seed nuclei: we assumed $\epsilon_d = 10^{-13}$, whereas Nanni et al. (2013) scale ϵ_d with the carbon excess with respect to oxygen (see session 4.1 in Nanni et al. 2013).

Turning to the metallicity of the new models presented here, $Z=4 \times 10^{-3}$, we see in the top, middle panels of Fig. 4 that the difference with Ferrarotti & Gail (2006) is smaller than for $Z=10^{-3}$. The models by Ferrarotti & Gail (2006) produce more dust for $M \geq 2.5M_{\odot}$; this is due to the different convective model adopted, because the use of the FST description partially limits the efficiency of TDU for the masses close to the limit for HBB.

For $Z=8 \times 10^{-3}$ the differences among the three compilations depends on the stellar mass. For $M \leq 2M_{\odot}$ our yields are a factor ~ 3 smaller compared to Ferrarotti & Gail (2006) and Nanni et al. (2013). These models experience a strong mass loss as soon as they become carbon stars, owing to the large sensitivity of the formulation by Wachter et al. (2008) to the effective temperature of the star, and the small temperatures typical of AGBs of this metallicity. Consequently, they loose their envelope very rapidly, preventing the possibility that large quantities of carbon are dredged-up to the surface. For masses above $\sim 2M_{\odot}$ the carbon dust produced by our models is similar to Nanni et al. (2013), and smaller than Ferrarotti & Gail (2006); this likely reflects the difference in the computation of the low-T opacities in the C-rich mixture, as discussed previously.

The amount of silicon carbide formed is independent of the surface carbon enrichment, because in this case silicon is the key-element. We see in the bottom panels of Fig. 4 that, independently of metallicity, more SiC is formed in our case, compared to Ferrarotti & Gail (2006) and Nanni et al. (2013). The reason for this is in the details of the growth of SiC and solid carbon grains in the winds of C-stars. SiC is formed in more internal regions, and is rather transparent to the radiation, thus determining only a modest acceleration of the wind. Carbon grains are formed in more external layers, and their large opacity favours a fast acceleration of the wind. The formation of carbon grains halts the growth of SiC grains, because the acceleration of the wind determines a drop in the density of silicon particles in the wind. In the models by Ferrarotti & Gail (2006) and Nanni et al. (2013) the amount of carbon formed is larger, which, in turn, determines a lower content of SiC.

5.3 Dust from C-stars: the trend with mass and metallicity

In the previous sections we stressed how dust production by C-stars is sensitive to many uncertainties, the most relevant being the treatment of convective borders and the description of mass loss.

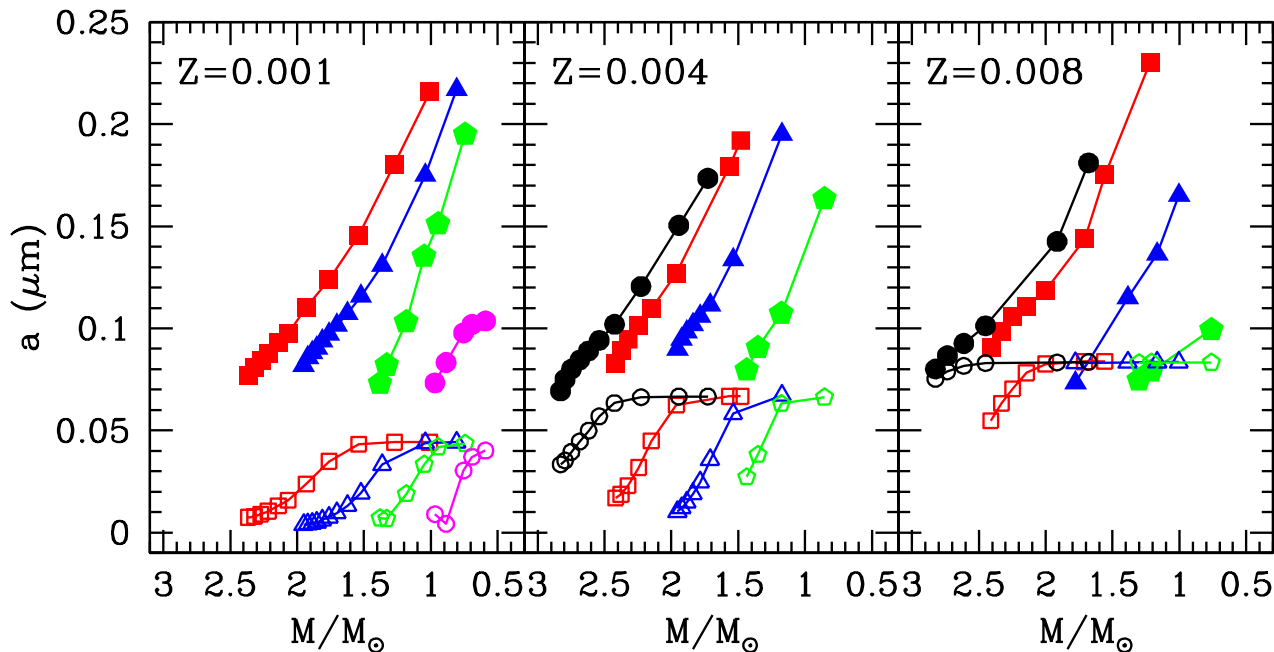


Figure 5. The variation of the size of dust grains of carbon (full points) and SiC (open) during the AGB evolution of models of metallicity $Z = 10^{-3}$ (left panel), $Z = 4 \times 10^{-3}$ (middle), $Z = 8 \times 10^{-3}$ (right). The initial masses are $3M_{\odot}$ (black circles), $2.5M_{\odot}$ (red squares), $2M_{\odot}$ (blue triangles), $1.5M_{\odot}$ (green pentagons). For the $Z = 10^{-3}$ metallicity we also show the $1M_{\odot}$ model (magenta circles).

We consider as our reference model the results obtained with the extra-mixing during the AGB phase calibrated as discussed in section 3.1, and the mass loss treatment modelled as in Wachter et al. (2008). These results are indicated as black, full circles in Fig. 2, 3, 4.

Fig. 5 shows the variation during the AGB life of the grain size of dust particles formed around stars of various masses and metallicities. Full points indicate the dimension of solid carbon grains, whereas open points refer to SiC. The choice of the current mass of the star as abscissa helps to understand how many grains of a given size are formed around the star during the whole evolution. Each point refers to the grain size in the middle of each interpulse phase. For the metallicities $Z = 4 \times 10^{-3}$ and $Z = 8 \times 10^{-3}$ we show results for models of initial masses 1.5, 2, 2.5, $3M_{\odot}$; in the $Z = 10^{-3}$ case, since the $3M_{\odot}$ model shows that HBB is active and that the C-star stage is not reached, we show the $1M_{\odot}$ case instead.

Concerning solid carbon, we see that for each mass the size of dust particles, a_C , increases during the evolution, owing to the increase in the surface carbon abundance and in the mass loss rate. Values of a_C span the range $0.07\text{--}0.2\text{ }\mu\text{m}$, although for masses $M \leq 1.5M_{\odot}$ we find $a_C \leq 0.1\text{ }\mu\text{m}$.

We see in the three panels of Fig. 2 that in the low-mass regime, with $M < 2M_{\odot}$, the amount of carbon dust formed increases with mass, independently of Z : the higher is M , the larger is the surface carbon enrichment. In this interval of mass the $Z = 10^{-3}$ models produce more carbon, because low- Z models experience deeper TDUs (Boothroyd & Sackmann 1988a), and reach more easily the C-star stage, owing to the smaller content of oxygen initially present at the surface.

For masses $M \geq 2M_{\odot}$ dust production is favoured in the higher metallicity models, because these evolve at smaller effective temperatures: dust formation occurs in layers closer to the stellar surface, where the densities are higher.

The mass of solid carbon produced, m_C , ranges from $10^{-4}M_{\odot}$ to $\sim 5 \times 10^{-3}M_{\odot}$ at $Z = 10^{-3}$, whereas at higher metallicities $m_C \sim 10^{-2}M_{\odot}$ for the two masses $M=2, 2.5M_{\odot}$.

In the three bottom panels of Fig. 5 we see that SiC grains grow during the evolution until a threshold size is reached, after which no further growth occurs. The maximum dimension achieved by SiC grains ranges from $\sim 0.05\text{ }\mu\text{m}$ for $Z = 10^{-3}$, to $\sim 0.07\text{ }\mu\text{m}$ for $Z = 4 \times 10^{-3}$, up to $\sim 0.09\text{ }\mu\text{m}$ for $Z = 8 \times 10^{-3}$.

This behaviour can be explained by the saturation due to the lack of silicon particles in the wind. Owing to the stability of SiS molecule, in carbon-rich environments we have $n_{\text{Si}} = [(1 - f_{\text{SiC}})\epsilon_{\text{Si}} - \epsilon_{\text{S}}]n_{\text{H}}$ (Ferrarotti & Gail 2006), where ϵ_{Si} and ϵ_{S} are the number density of silicon and sulphur particles in the wind (normalized to the hydrogen density), whereas f_{SiC} is the fraction of silicon condensed into SiC. This expression poses an upper limit on the amount of SiC that can form, corresponding to the value of f_{SiC} at which n_{Si} vanishes:

$$f_{\text{SiC}} = 1 - \frac{\epsilon_{\text{S}}}{\epsilon_{\text{Si}}}$$

Because in solar or α -enhanced mixtures $\frac{\epsilon_{\text{S}}}{\epsilon_{\text{Si}}} \sim 0.4$ (Grevesse & Sauval 1998), f_{SiC} cannot exceed $\sim 60\%$.

The mass of SiC (m_{SiC}) produced increases with the stellar mass, as can be seen in Fig. 3, because of the larger

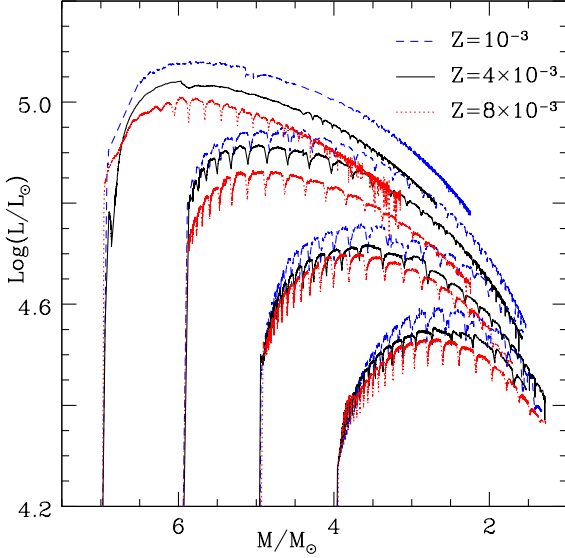


Figure 6. The AGB evolution of the luminosity of models of initial mass $M \geq 4M_{\odot}$ for the metallicities $Z = 10^{-3}$ (blue, dashed lines), $Z = 4 \times 10^{-3}$ (black, solid) and $Z = 8 \times 10^{-3}$ (red, dotted track).

mass returned into the interstellar medium by massive AGBs during the evolution. Higher-metallicity models produce more SiC, owing to the larger amount of silicon present in the stars. $Z = 10^{-3}$ models produce an amount of SiC $10^{-5}M_{\odot} < m_{\text{SiC}} < 10^{-4}M_{\odot}$, whereas at $Z = 4 \times 10^{-3}$ we find $5 \times 10^{-5}M_{\odot} < m_{\text{SiC}} < 5 \times 10^{-4}M_{\odot}$; the largest production of SiC occurs at $Z = 8 \times 10^{-3}$, for which we have $10^{-4}M_{\odot} < m_{\text{SiC}} < 10^{-3}M_{\odot}$. The scaling of the mass of SiC produced with the metallicity is approximately linear, as expected.

6 THE EFFECTS OF HOT BOTTOM BURNING ON MASSIVE MODELS

Stellar models with mass above $\sim 3M_{\odot}$ experience HBB during the interpulse phases of the AGB evolution. The key-parameter to describe the HBB strength is the temperature at the bottom of the convective envelope, which determines the degree of nucleosynthesis experienced in those regions, and the modification of the surface chemistry. Stars that experience HBB reach very high luminosities (Blöcker & Schönberner 1991), much larger than predicted by the classic relation by Paczynski (1970).

Fig. 6 shows the evolution of the luminosity of AGB models of various initial masses and metallicities.

The luminosity first increases in the early AGB phases, then declines until the envelope is consumed. The initial trend is due to the increase in the core mass of the star, whereas the consumption of the envelope is the reason for the later decrease in the overall energy flux.

Higher mass models evolve on bigger cores, experience stronger HBB, and evolve at larger luminosities.

Models with smaller metallicity are sustained by a more powerful CNO-burning shell: HBB conditions are reached more easily in lower Z models, that evolve at larger

luminosities. We see in Fig. 6 that for a given mass the $Z = 4 \times 10^{-3}$ models (hereinafter z4m3, see Ventura et al. (2013b) for a more exhaustive discussion of the physical properties of AGB models with $Z = 4 \times 10^{-3}$) presented here evolve at a luminosity intermediate between models of the same mass of metallicity $Z = 10^{-3}$ (hereinafter z1m3) and $Z = 8 \times 10^{-3}$ (z8m3).

The evolution of the surface chemistry of massive AGBs can also be explained on the basis of the HBB experienced. Fig. 7 shows the variation of the surface abundances of oxygen (solid tracks) and carbon (dotted lines) for the same models shown in Fig. 6.

The strong depletion of the surface carbon in the early AGB phases is the signature of HBB, starting at $\sim 40\text{MK}$. The depletion of oxygen requires higher temperatures at the bottom of the convective zone ($T_{\text{bce}} \sim 70\text{MK}$), thus it takes place in more advanced phases. The z8m3 models experience a soft HBB, thus the reduction of the surface oxygen is modest (at most a factor ~ 2). In the z1m3 models the depletion of the surface oxygen is not monotonic with mass: stars with mass around $\sim 6M_{\odot}$ produce the most O-poor ejecta, the initial oxygen being destroyed by almost two orders of magnitude. More massive stars, though experiencing a stronger HBB, lose their surface envelope very rapidly, before a very advanced nucleosynthesis can be activated: their surface oxygen is slightly higher (Ventura & D’Antona 2011; Ventura et al. 2013a).

In all the cases shown in Fig. 7 we see that the surface C/O keeps below unity, thus preventing the possibility that the C-star stage is reached, and, consequently, that carbon-type dust is formed.

The size of the dust grains of the various species that form during the AGB evolution is shown in the three panels of Fig. 8. For clarity reasons we show only the $4M_{\odot}$ and $7.5M_{\odot}$ cases, as representative of the lowest and highest masses experiencing HBB.

In agreement with previous investigations, we find that olivine is the dominant species (Ferrarotti & Gail 2006). For the z4m3 and z8m3 cases the dimension of the olivine grains formed increases with the stellar mass. The grain size a_{ol} is in the range $0.07\mu\text{m} < a_{\text{ol}} < 0.13\mu\text{m}$ for $Z = 8 \times 10^{-3}$, and $0.06\mu\text{m} < a_{\text{ol}} < 0.11\mu\text{m}$ for $Z = 4 \times 10^{-3}$. The z4m3 produce smaller amounts of olivine than their z8m3 counterparts, because although they evolve at larger luminosities and lose mass at a higher rate, their surface silicon (which scales with the metallicity, and is scarcely touched by HBB) is smaller. The z1m3 models produce even less olivine, a_{ol} never exceeding $\sim 0.07\mu\text{m}$. The formation of olivine grains in the more massive models of this metallicity stops at a certain stage during the AGB evolution, because the strong depletion of the surface oxygen (see the left panel of Fig. 7) prevents the formation of water molecules, that are essential to form olivine grains. This behaviour was found and discussed in Ventura et al. (2012a).

In the winds of M-stars pyroxene is the second most abundant species after olivine. Depending on the metallicity, the size of pyroxene grains ranges from $\sim 0.04\mu\text{m}$ to $\sim 0.07\mu\text{m}$ (see Fig. 8).

Quartz is the least abundant among the silicates, the grain size keeping below $\sim 0.04\mu\text{m}$. Note that in the early AGB phases the size of quartz grains is larger: this is because a smaller amount of olivine is formed, thus the acceleration

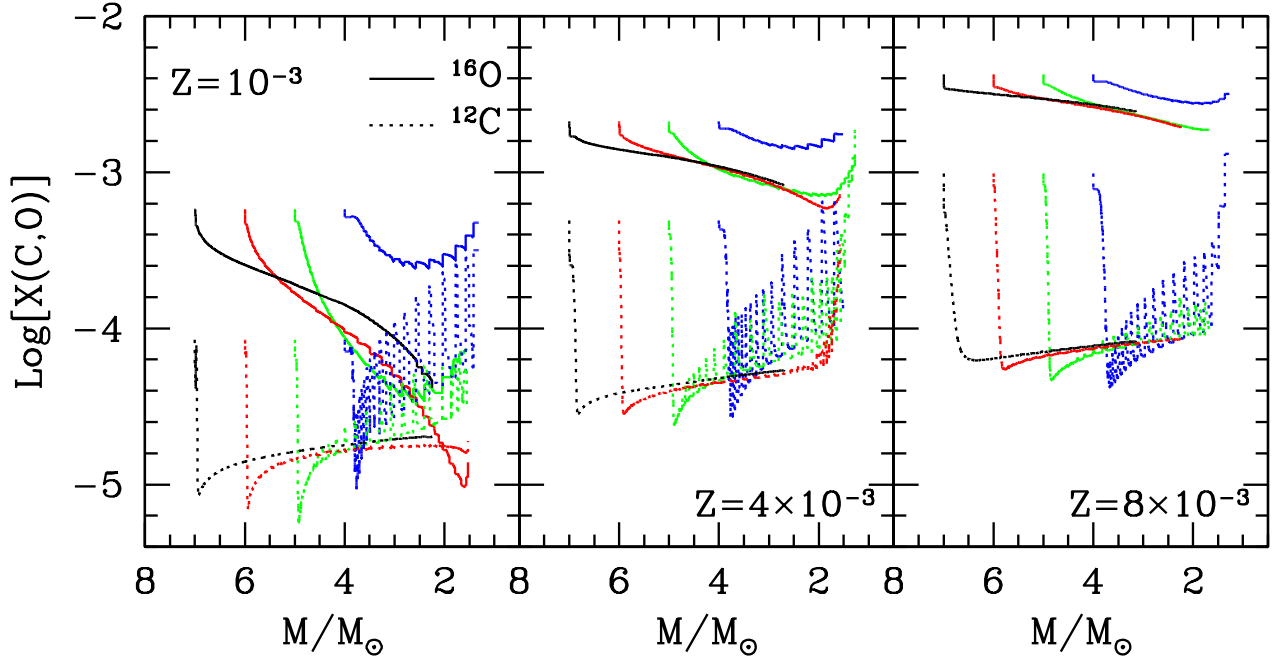


Figure 7. The evolution of the the surface mass fraction of carbon (dotted lines) and oxygen (solid tracks) in models of initial mass in the range $4 - 8 M_{\odot}$ of metallicity $Z = 10^{-3}$ (left), $Z = 4 \times 10^{-3}$ (middle) and $Z = 8 \times 10^{-3}$ (right). The different colors correspond to masses $7 M_{\odot}$ (black), $6 M_{\odot}$ (red), $5 M_{\odot}$ (green), $4 M_{\odot}$ (blue).

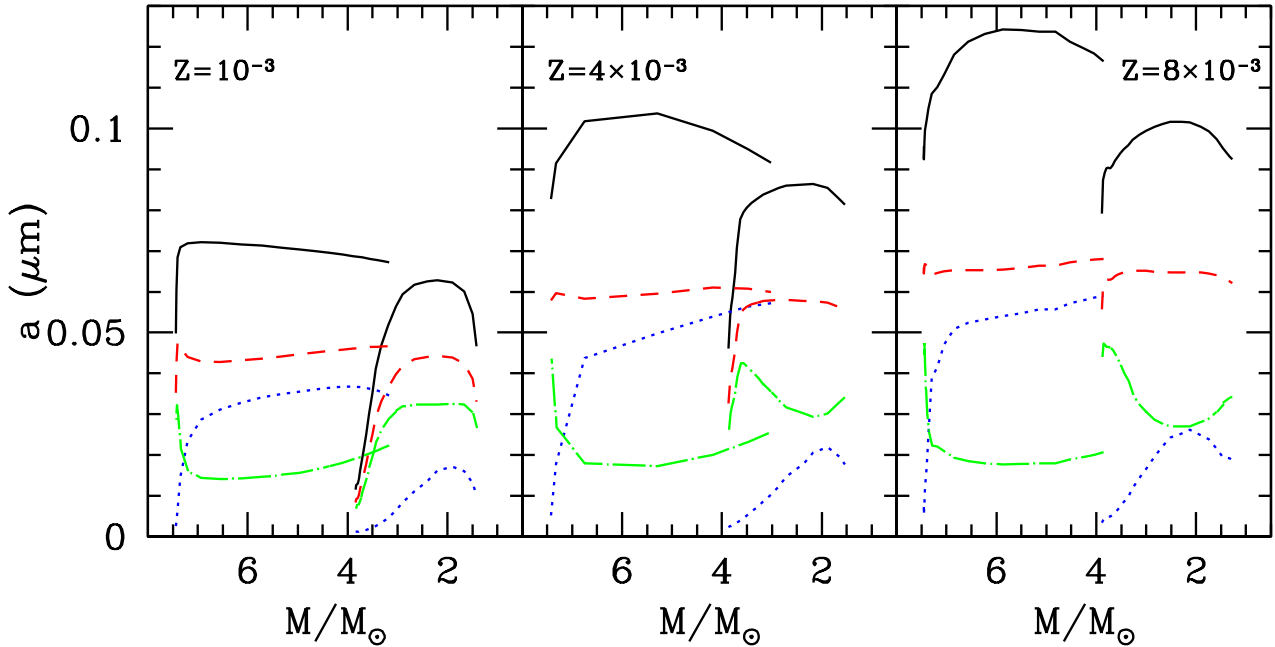


Figure 8. The variation of the grains size of olivine (black, solid lines), pyroxene (red, dashed), quartz (green, dot-dashed) and corundum (blue, dotted) in models of initial mass $4 M_{\odot}$ and $7.5 M_{\odot}$ of metallicity $Z = 10^{-3}$ (left), $Z = 4 \times 10^{-3}$ (middle) and $Z = 8 \times 10^{-3}$ (right).

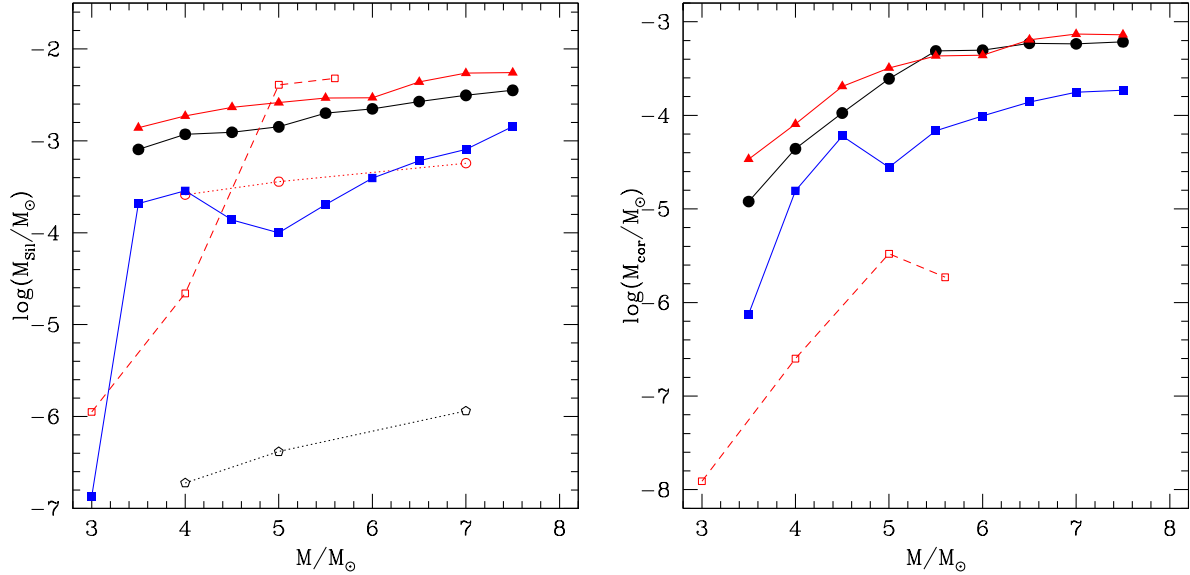


Figure 9. Left: The mass of silicates produced as a function of the initial mass for the metallicities $Z = 8 \times 10^{-3}$ (red, solid triangles), $Z = 4 \times 10^{-3}$ (black, full circles), $Z = 10^{-3}$ (blue, full squares). Open points refer to results from Ferrarotti & Gail (2006) of metallicity $Z = 8 \times 10^{-3}$ (red, open circles) and $Z = 4 \times 10^{-3}$ (black, open circles); these results are connected with dotted lines. Open squares (connected with a dashed line) refer to results from Nanni et al. (2013), of metallicity $Z = 8 \times 10^{-3}$. Right: The mass of corundum produced by massive AGBs. The meaning of the symbols is the same as in the left panel.

experienced by the wind is smaller, which contributes to form more quartz.

Besides silicates, an additional species that forms in the winds of M-stars is corundum, an Al-rich compound very stable (Sharp & Huebner 1990), and extremely transparent to radiation (Koike et al. 1995). In our previous investigations the formation of corundum was neglected, although, owing to its stability, it is likely that considerable amounts of this dust species form in regions close to the surface of the star (Gail & Sedlmayr 1998). The details of the corundum condensation process and a discussion of the related uncertainties, will be published in a separate paper (Dell’Agli et al., submitted).

The variation of the corundum grain size during the AGB evolution is different compared to silicates: corundum particles form in larger and larger dimensions as the evolution proceeds, whereas the size of silicates follows the path traced by luminosity (see Fig. 6 and 8). This is an effect of HBB, which, via activation of the Mg–Al nucleosynthesis, favours a gradual aluminium enrichment of the surface layers (Ventura et al. 2013a).

The total mass of silicates and corundum is shown in Fig. 9. For the metallicities $Z = 4 \times 10^{-3}$ and $Z = 8 \times 10^{-3}$ the mass of silicates produced is in the range $10^{-3}M_{\odot} < M_{\text{sil}} < 10^{-2}M_{\odot}$ and increases with the stellar mass, in agreement with the previous discussion on the grain sizes of olivine and pyroxene. The z1m3 models produce a smaller quantity of dust, owing to the scarcity of silicon available, but also because of the strong depletion of the surface oxygen: this is the reason for the dip around $\sim 5M_{\odot}$, that can be seen in the z1m3 line in the left panel of Fig. 9.

The comparison with the results by Ferrarotti & Gail (2006) shows that the mass of silicates produced by our

models is much larger, owing to the stronger HBB experienced, which, in turn, favours a large increase in the mass rate, hence in the density of the wind. This is particularly evident at the small metallicities, where the production of dust by the Ferrarotti & Gail (2006) is modest, as a consequence of the scarcity of silicon in the surface layers of the star (the models by Ferrarotti & Gail (2006) of metallicity $Z = 10^{-3}$ are not shown in the figure, as they would fall off the chosen scale for the vertical axis).

The comparison with the results by Nanni et al. (2013) is less straightforward. At $Z = 8 \times 10^{-3}$ the overall mass of silicates produced by our models is larger, though the two most massive models in the Nanni et al. (2013) compilation produce a quantity of silicates comparable to ours. In the $Z = 10^{-3}$ case no silicates is produced by Nanni et al. (2013) models, because the models, though experiencing a soft HBB, eventually become carbon stars, thus produce carbon-type dust.

A word of caution is needed here. In the models presented here we follow the same schematization described in Ferrarotti & Gail (2006), in that we assume that the disintegration of olivine, and more generally of silicates, takes place by chemisputtering: Gail & Sedlmayr (1999) discuss the stability of silicates, arguing against the possibility that pure thermal composition is responsible for the disintegration of silicates. This assumption is compatible with the silicates forming reactions given in Tab. 4.2. Conversely, Nanni et al. (2013) assume that the destruction of silicates grains is triggered by a pure vaporization process. The difference between these two descriptions is that while in the chemisputtering case silicates are not stable at temperatures above $\sim 1100\text{K}$, in the second hypothesis this threshold is lifted to $\sim 1500\text{K}$. Clearly in the latter case more sili-

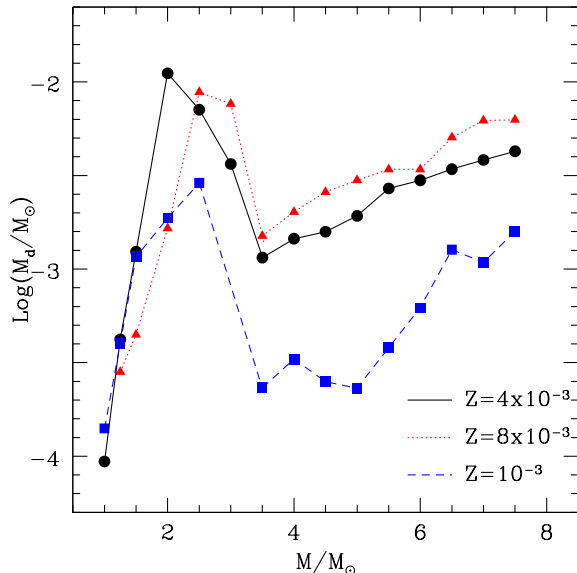


Figure 10. The mass of dust produced by AGB models of various initial mass. The various symbols refer to the metallicities $Z = 10^{-3}$ (blue squares), $Z = 4 \times 10^{-3}$ (black circles) and $Z = 8 \times 10^{-3}$ (red triangles).

cates are formed, because the condensation process begins in regions closer to the surface of the star, at larger densities. Discriminating among these two hypothesis is beyond the scope of the present investigation, however we are more favourable to the chemisputtering solution because: a) condensation temperatures for silicates as high as 1500K are not observed in radiative transfer models for O-rich circumstellar dust shells (Groenewegen et al. 2009); b) observationally, the highest temperatures observed are ~ 1350 K for aluminum dust (Karovikova et al. 2013).

The mass of corundum produced, m_{co} , is also increasing with the stellar mass (see right panel of Fig. 9). Because of the saturation conditions reached, there is practically no difference between the $Z = 4 \times 10^{-3}$ models and their $Z = 8 \times 10^{-3}$ counterparts: m_{co} varies from a few $10^{-6} M_{\odot}$ for $M = 3.5 M_{\odot}$, to $\sim 10^{-3} M_{\odot}$ for $M = 7.5 M_{\odot}$. The $Z = 10^{-3}$ models produce a smaller amount of corundum, owing to the low surface mass fraction of aluminium.

7 CONCLUSIONS

In the previous sections we discussed separately the dust yields by stars with mass $M < 3 M_{\odot}$, that produce carbon dust, and by more massive AGBs, that produce silicates. TDU favours the surface carbon enrichment for the lower masses, where HBB dominates for masses above $3 M_{\odot}$.

The total dust produced by stars of various masses and metallicities is shown in Fig. 10. For consistency with the new grid of AGB models with $Z = 4 \times 10^{-3}$ presented here, the mass of carbon dust produced by $Z = 10^{-3}$ and $Z = 8 \times 10^{-3}$ (discussed in Ventura et al. 2012a,b) have been recalculated to account for: i) a small extra-mixing from the bottom of the convective envelope and ii) the mass loss rate by Wachter et al. (2008), that is more suitable to describe mass loss for carbon stars. Both these effects increase the

quantity of carbon-dust formed around $M < 3 M_{\odot}$ AGBs. The extra-mixing below the base of the envelope favours a more penetrating TDU, thus a higher surface carbon available. Use of the Wachter et al. (2008) mass loss leads to higher rates for carbon stars; this, in turn, determines an increase in the density of the wind, and consequently a higher rate of dust formation.

The quantity of dust formed depends on the initial mass of the star. The various lines in Fig. 10, indicating different metallicities, outline an initial increasing trend for masses $M < 2 - 2.5 M_{\odot}$, owing to the higher number of TPs experienced, which favour a larger carbon enrichment of the surface layers. In these stars $\sim 80 - 90\%$ of dust is under the form of solid carbon, with $\sim 10 - 20\%$ of SiC and solid iron.

The stars with mass around $3.5 M_{\odot}$ produce smaller quantities of dust, because HBB prevents the formation of carbon-type dust, and their mass loss rates are not sufficiently large to trigger the formation of large amount of silicates.

Higher mass models produce more dust, because they evolve at larger luminosities, thus they loose mass at larger rates. Most of the dust produced ($\sim 80\%$) are silicates (mostly olivine), with traces of cordundum and iron.

The yields scale with the metallicity in the high-mass domain, owing to the quantity of silicon available, which increases with Z .

In the low-mass domain, where carbon dust formation occurs, the results are less sensitive to metallicity. The overall dust produced by the $Z = 10^{-3}$ models is smaller, because the minimum mass at which HBB occurs is smaller, which limits the range of masses experiencing carbon enrichment.

ACKNOWLEDGMENTS

RS acknowledges that the research leading to these results has received funding from the European Research Council under the European Unions Seventh Framework Programme (FP/2007-2013) / ERC Grant Agreement n. 306476. The authors are indebted to the anonymous referee, for the careful reading of the manuscript, that helped improving the quality of this work.

REFERENCES

- Bertschinger E., Chevalier R. A. 1985, ApJ, 167, 190
- Bessel M. S., Wood P. R., Evans T. L., 1983, MNRAS, 202, 59
- Blöcker T., 1995, A&A, 297, 727
- Blöcker T., Schönberner D., 1991, A&A, 244, L43
- Boothroyd A. I., Sachmann, I. J. 1988a, ApJ, 328, 653
- Boothroyd A. I., Sachmann, I. J. 1988b, ApJ, 328, 671
- Bowen G. H., 1988, ApJ, 329, 299
- Bressan A., Marigo P., Girardi L., Salasnich B., Dal Cero C., Rubele S., Nanni A., 2012, MNRAS, 427, 127
- Briquet M., Morel T., Thoul A., Scuflaire R., Miglio A., Montalbán J., Dupret, M. A., Aerts C., 2007, MNRAS, 381, 1482
- Canuto V.M.C., Mazzitelli I., 1991, ApJ, 370, 295

- Carretta E., Bragaglia A., Gratton R., D’Orazi V., Lucatello S., 2009, *A&A*, 508, 695
- Claret A., 2007, *A&A*, 475, 1019
- Cloutman L.D., Eoll J.G., 1976, *ApJ*, 206, 548
- D’Ercole A., Vesperini E., D’Antona F., Mc Millan S.L.W., Recchi S., 2008, *MNRAS*, 391, 825
- D’Ercole A., D’Antona F., Ventura P., Vesperini E., Mc Millan S.L.W., 2010, *MNRAS*, 407, 854
- Di Criscienzo M., Dell’Agli F., Ventura P., Schneider R., Valiante R., La Franca F., Rossi C., Gallerani S., Maiolino R., 2013, *MNRAS*, 433, 313
- Dwek, E., Galliano, F. & Jones, O., 2007, *ApJ*, 662, 927D
- Ferrarotti A.D., Gail H.P., 2001, *A&A*, 371, 133
- Ferrarotti A.D., Gail H.P., 2002, *A&A*, 382, 256
- Ferrarotti A.D., Gail H.P., 2006, *A&A*, 553, 576
- Fleischer A. J., Gauger A., Sedlmayr E., 1992, *A&A*, 266, 339
- Gail H. P., Sedlmayr E., 1985, *A&A*, 148, 183
- Gail H.P., Sedlmayr E., 1998, *Faraday Discussions*, 109, 303
- Gail H. P., Sedlmayr E., 1999, *A&A*, 347, 594
- Golub G. H., Ortega J. M., 1992, *Scientific Computing and Differential Equations* (Boston: Academic Press)
- Gratton R., Carretta E., Bragaglia A. 2012, *AR&Av*, 20, 50
- Grevesse N., Sauval A. J., 1998, *SSrv*, 85, 161
- Groenewegen M. A. T., 2004, *A&A*, 425, 595
- Groenewegen M. A. T., Whitelock P. A., Smith C. H., Kerschbaum F., 1998, *MNRAS*, 293, 18
- Groenewegen M. A. T., Sloan G. C., Soszynski I., Petersen E. A., 2009, *A&A*, 506, 1277
- Herwig F., 2000, *A&A*, 360, 952
- Herwig F., 2005, *AR&A*, 43, 435
- Herwig F., Austin S.M., 2004, *ApJ*, 613, L73
- Iben I. Jr, Renzini A., 1983, *ARA&A*, 21, 271
- Iglesias C. A., Rogers F. J., 1996, *ApJ*, 464, 943
- Izzard R. G., Tout C. A., Karakas A. I., Pols O. R., 2004, *MNRAS*, 350, 407
- Karakas A. I., Lattanzio J. C., Pols O. R., 2002, *PASA*, 19, 515
- Karakas A. I., 2011, in *ASP Conf. Ser.*, Why Galaxies Care about AGB Stars II: Shining Examples and Common Inhabitants. Proceedings of a conference held at University Campus, Vienna, Austria, 16-20 August 2010. Edited by F. Kerschbaum, T. Lebzelter, and R. F. Wing. San Francisco: Astronomical Society of the Pacific, 2011., 455, p.3
- Karovicova I., Wittkowski M., Ohnaka K., Boboltz D. A., Fossat E., Scholz M. 2013, *A&A*, 560, A75
- Knapp G. R. 1985, *ApJ*, 293, 273
- Koike C., Kaito C., Yamamoto T., Shibai H., Kimura S., Suto H., 1995, *Icarus*, 114, 203
- Larsen S. S., Clausen J. V., Storm J., 2000, *A&A*, 364, 455
- Lattanzio J. C., Boothroyd A. I., 1997. In *Astrophysical implications of the laboratory study of presolar materials*, ed. T. Bernatowitz, E. Zinner, AIP Conf. Ser. 85
- Lucy L. B., 1976, *ApJ*, 205, 482
- Marigo P., 2002, *A&A*, 387, 507
- Marigo P., Girardi L., 2007, *A&A*, 469, 239
- Marigo P., Aringer B., 2009, *A&A*, 508, 1538
- Marigo P., Girardi L., Bressan A., 1999, *A&A*, 344, 123
- Mattsson L., Wahlin R., Höfner S., Eriksson K., 2008, *A&A*, 484, L5
- Montalbán J., Miglio A., Noels A., Dupret, M. A., Scuflaire R., Ventura P., 2013, *ApJ*, 766, 118
- Mowlavi N., 1999, *A&A*, 350, 73
- Nanni A., Bressan A., Marigo P., Girardi L., 2013, *MNRAS*, 434, 2390
- Ossenkopf V., Henning Th., Mathis J. S., 1992, *A&A*, 261, 567
- Paczynski B., 1970, *Acta Astron.*, 20, 47
- Piotto G., in *IAU Symp.* 258, 2009, The ages of stars, ed. E. E. Mamajek, D. R. Soderblom, R. F. G. Wyse (Cambridge: Cambridge University Press), 233
- Renzini A., Voli M., 1981, *A&A*, 94, 175
- Sharp C. M., Huebner W. F., 1990, *ApJS*, 72, 417
- Straniero O., Chieffi A., Limongi M., Busso M., Gallino R., Arlandini C., 1997, *ApJ*, 478, 332
- Ventura P., D’Antona F., Mazzitelli I., Gratton R., 2001, *ApJ*, 550, L65
- Ventura P., Carini R., D’Antona F., 2011, *MNRAS*, 415, 3865
- Ventura P., D’Antona F., 2005a, *A&A*, 431, 279
- Ventura P., D’Antona F., 2005b, *A&A*, 439, 1075
- Ventura P., D’Antona F., 2009, *MNRAS*, 499, 835
- Ventura P., D’Antona F., 2011, *MNRAS*, 410, 2760
- Ventura P., Di Criscienzo M., Schneider R., Carini R., Valiante R., D’Antona F., Gallerani S., Maiolino R., Tornambé A., 2012a, *MNRAS*, 420, 1442
- Ventura P., Di Criscienzo M., Schneider R., Carini R., Valiante R., D’Antona F., Gallerani S., Maiolino R., Tornambé A., 2012b, *MNRAS*, 424, 2345
- VandenBerg, D. A., Bergbusch P. A., Dowler P. D., 2006, *ApJS*, 162, 375
- Ventura P., Marigo P., 2009, *MNRAS*, 399, L54
- Ventura P., Marigo P., 2010, *MNRAS*, 408, 2476
- Ventura P., D’Antona F., Mazzitelli I., 2000, *A&A*, 363, 605
- Ventura P., Zepieri A., Mazzitelli I., D’Antona F., 1998, *A&A*, 334, 953
- Ventura P., Di Criscienzo M., Carini R., D’Antona F., 2013a, *MNRAS*, 431, 3642
- Ventura P., Di Criscienzo M., D’Antona F., Vesperini E., D’Ercole A., Tailo M., Dell’Agli F., 2013b, *MNRAS*, in press
- Wachter A., Schröder K. P., Winters J. M., Arndt T. U., Sedlmayr E., 2002, *A&A*, 384, 452
- Wachter A., Winters J. M., Schröder K. P., Sedlmayr E., 2008, *A&A*, 486, 497
- Wallerstein G., Knapp G. R., 1998, *ARA&A*, 36, 369
- Wood P. R., 1979, *ApJ*, 227, 220